Thermochimica Acta, 199 (1992) 45–55
Elsevier Science Publishers B.V., Amsterdam

Temperature-programmed desorption of H_2S from alkali-metal zeolites [1]

I. Ferino, R. Monaci, E. Rombi, V. Solinas and L. Burlamacchi

Dipartimento di Scienze Chimiche, Università di Cagliari, Via Ospedale 72, 09124 Cagliari (Italy)

(Received in final form 6 September 1991)

Abstract

The temperature-programmed desorption (TPD) of H_2S from X zeolites containing various amounts of Cs^+ and Rb^+ ions has been investigated. The TPD behaviour of some zeolites with different Si/Al ratios has also been studied. The role of the operating conditions during the saturation step is considered. The results are discussed in terms of the acid–basic character of the solid, which seems to determine the H_2S adsorption mode.

INTRODUCTION

The adsorption of H_2S on alkali-metal zeolites is a key step in H_2S oxidation by SO_2 or O_2 [1–7] and in CH_3OH conversion to CH_3SH and $(CH_3)_2S$ [8].

A similar situation also seems to occur in the case of 2-methylfuran (MF) conversion to 2-methylthiophene (MT). This has been studied in our laboratory [9–12] because of the importance of the main reaction product as an intermediate in pharmaceutical synthesis. The reaction was found to require the simultaneous presence on the catalyst of acid–base pairs [10]. These were identified as the alkali-metal cations and the lattice oxygens of the zeolite respectively [11]. A general picture of the reaction between H_2S and MF over Me^INa-faujasites (with Me^I = Li, Na, K, Rb and Cs) has been proposed [11,12]. A radical mechanism occurs on these catalysts parallel to the main ionic mechanism. Their competition was found to be related to the basic strength of the zeolite sites as measured from the partial charge resting on the lattice oxygens, δ_O. Lower (absolute) δ_O values enhance the selectivity to radical byproducts. The highest selectivity is displayed by LiNaY and NaY. Ionic reactions are favoured by high (absolute) δ_O values,

Correspondence to: I. Ferino, Dipartimento di Scienze Chimiche, Università di Cagliari, Via Ospedale 72, 09124 Cagliari, Italy.

[1] Presented at the 12th National Conference on Calorimetry and Thermal Analysis, Bari, Italy, 11–13 December 1990.

the best selectivity, however, being observed for CsNaY, LiNaX and NaX, i.e. catalysts with an optimum balance between the strength of basic (lattice oxygens) and acid sites (cations).

Conversion of MF through ionic mechanisms requires Brönsted acidity. This is thought to be initiated by ionic dissociative adsorption of H_2S induced by the negative charge of the oxygen atoms. Particular attention should thus be paid to the type of interaction path between H_2S and Me^INa-faujasites. It seems that useful information can be obtained by temperature-programmed desorption (TPD). Preliminary results [9] indicate that Me^INaY zeolites behave differently from Me^INaX with respect to H_2S adsorption.

The results of a TPD investigation on CsNaX and RbNaX systems with different degrees of ion exchange are presented here. H_2S desorption from NaY, NaΩ and silicalite was also recorded. A few runs concerning the TPD of MF from some selected X zeolites were performed.

EXPERIMENTAL

Zeolites

NaX, NaY and NaΩ were commercial products from Union Carbide (Na13X, LZY-52 and ELZ Ω). Silicalite was kindly supplied by Prof. L. Forni (University of Milan). CsNaX and RbNaX zeolites were prepared from the original NaX by ion exchange with CsCl and RbCl solutions of appropriate concentrations, depending on the amount of alkali-metal ion to be introduced. Refluxing for several hours at 353 K was needed to achieve the highest degree of ion exchange. Washing in distilled water, drying at 383 K and calcining in air at 773 K followed. The same procedure was used to prepare the highly exchanged KNaX sample. All reagents were Fluka analytical grade products.

The chemical composition of the samples (Table 1) was determined by atomic adsorption spectrometry on the solution obtained after attack of the solid with a hot $HF/HClO_4$ mixture (1 : 1 by volume).

TPD runs

TPD was performed on a conventional apparatus, equipped with a quartz microreactor (1 cm internal diameter) and a Philips thermocoax miniature thermocouple. A thermal conductivity detector was used. Briefly, a weighed amount of the sample (about 150 mg) was placed into the reactor and activated in flowing helium (40 $cm^3\ min^{-1}$) for 2 h at 873 K (heating rate 10 K min^{-1}). After cooling to 423 K, H_2S was admitted (5 $cm^3\ min^{-1}$) and kept flowing for 30 min. The sample was then purged in helium (12 h at 423 K, 40 $cm^3\ min^{-1}$) before starting the TPD run. As too

TABLE 1

Characteristics of the zeolites employed

Sample	Chemical composition	δ_O [a]
NaX	$Na_{80}(AlO_2)_{80}(SiO_2)_{112}$	−0.399
NaY	$Na_{55}(AlO_2)_{55}(SiO_2)_{137}$	−0.349
NaΩ	$Na_8(AlO_2)_8(SiO_2)_{28}$	−0.319
Silicalite	$(SiO_2)_{96}$	
Cs_5NaX	$Cs_5Na_{75}(AlO_2)_{80}(SiO_2)_{112}$	−0.403
$Cs_{12}NaX$	$Cs_{12}Na_{68}(AlO_2)_{80}(SiO_2)_{112}$	−0.411
$Cs_{26}NaX$	$Cs_{26}Na_{54}(AlO_2)_{80}(SiO_2)_{112}$	−0.435
$Cs_{35}NaX$	$Cs_{35}Na_{45}(AlO_2)_{80}(SiO_2)_{112}$	−0.460
Rb_3NaX	$Rb_3Na_{77}(AlO_2)_{80}(SiO_2)_{112}$	−0.402
Rb_6NaX	$Rb_6Na_{74}(AlO_2)_{80}(SiO_2)_{112}$	−0.403
$Rb_{28}NaX$	$Rb_{28}Na_{52}(AlO_2)_{80}(SiO_2)_{112}$	−0.417
$Rb_{38}NaX$	$Rb_{38}Na_{42}(AlO_2)_{80}(SiO_2)_{112}$	−0.435
$K_{70}NaX$	$K_{70}Na_{10}(AlO_2)_{80}(SiO_2)_{112}$	−0.481

[a] Average charge on oxygen (see text).

low values of the heating rate make it difficult to distinguish individual peak maxima in the spectrum, heating was performed at 10 K min^{-1}. An upper temperature limit of 873 K was chosen in order to approach a desorption as complete as possible without loss of crystallinity of the zeolitic structure. Both helium and H_2S were of the highest commercially available purity (> 99.9999% and 99.5% respectively) and were further purified by means of cold traps filled with 13X molecular sieves, that were periodically regenerated by heating in air at 773 K overnight.

This procedure was occasionally changed to check the influence of the H_2S flow rate, time and temperature of the saturation step, and temperature of the purge step (for details see the Results section of this paper).

TPD of MF was performed on the same apparatus. After the usual activation the sample was contacted (for 30 min at 423 K) with flowing helium (5 cm^3 min^{-1}) previously bubbled through a saturator filled with liquid MF (Fluka analytical grade) at 323 K. Purging in helium (40 cm^3 min^{-1}) at 423 K for 12 h preceded the TPD run (heating rate 10 K min^{-1}, upper temperature limit 623 K).

RESULTS AND DISCUSSION

TPD of H_2S

The TPD spectra of the sodium forms of X, Y and Ω zeolites are reported in Fig. 1. The single peak present in each curve is symmetric for X and Y samples, whereas some tailing appears in the case of NaΩ. Further-

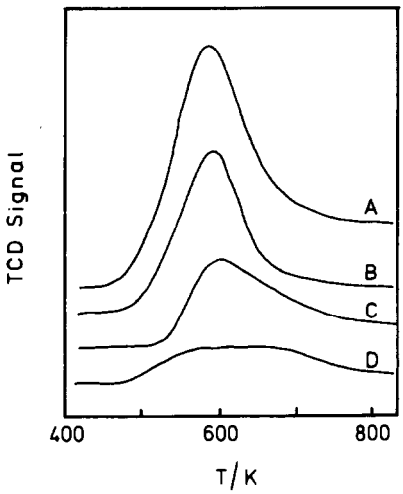

Fig. 1. TPD spectra of H_2S for (A) NaX, (B) NaY, (C) NaΩ and (D) silicalite (recording sensitivity×4). Saturation in flowing H_2S (5 cm^3 min^{-1}) during 30 min at 423 K. Purging in flowing helium (40 cm^3 min^{-1}) for 12 h at 423 K.

more, a very enlarged desorption line is observed on the silicalite sample, which is also shown in Fig. 1.

The spectra for the CsNaX and RbNaX series (Fig. 2) show that the curve for the original NaX sample (included in Fig. 2 for the sake of

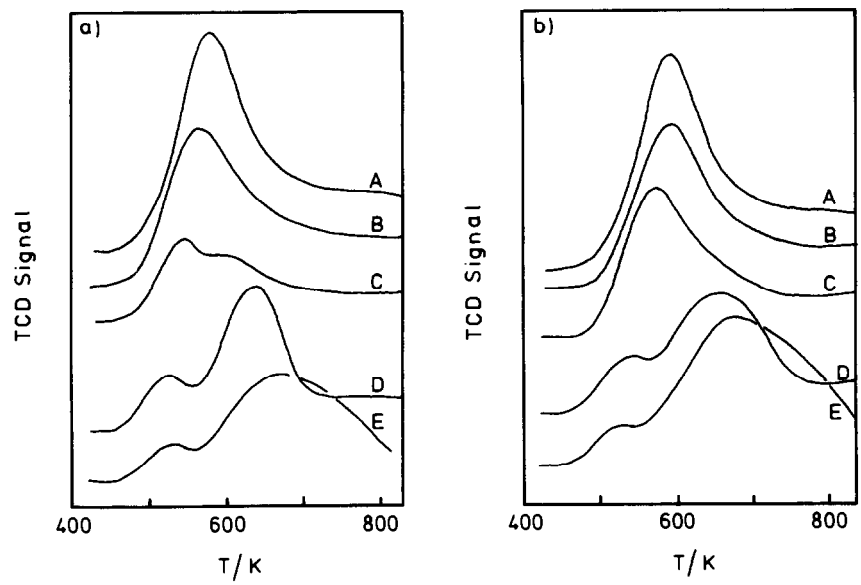

Fig. 2. (a) TPD spectra of H_2S for (A) NaX, (B) Cs_5NaX, (C) $Cs_{12}NaX$, (D) $Cs_{26}NaX$ and (E) $Cs_{35}NaX$; saturation and purging as in Fig. 1. (b) TPD spectra of H_2S for (A) NaX, (B) Rb_3NaX, (C) Rb_6NaX, (D) $Rb_{28}NaX$ and (E) $Rb_{38}NaX$; saturation and purging as in Fig. 1.

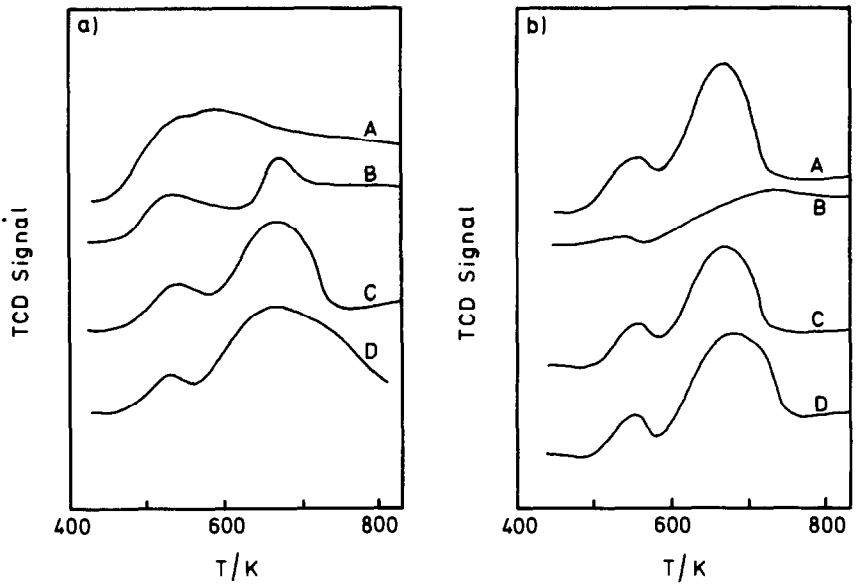

Fig. 3. (a) TPD spectra of H_2S for $Cs_{35}NaX$ after saturation at 423 K for (A) 5 min in H_2S at 40 cm^3 min^{-1}, (B) 5 min in H_2S at 5 cm^3 min^{-1}, (C) 30 min in H_2S at 40 cm^3 min^{-1} and (D) 30 min in H_2S at 5 cm^3 min^{-1}; purging as in Fig. 1. (b) TPD spectra of H_2S for $Cs_{26}NaX$ after saturation and purging at (A) 423 K, (B) 523 K, (C) 523 K (saturation) and 423 K (purging) and (D) 623 K (saturation) and 423 K (purging). H_2S flow rate and duration 5 cm^3 min^{-1} and 30 min.

completeness) progressively changes as the caesium content increases. For Cs_5NaX there is only a decrease in the area under the curve as opposed to the sharp NaX peak, together with a slight shift of its maximum towards lower temperatures. With $Cs_{12}NaX$, $Cs_{26}NaX$ and $Cs_{35}NaX$, a strong modification of the spectrum occurs: two peaks appear, and the second one is wider and has its maximum at high temperature. A similar trend is observed for the RbNaX series.

The H_2S flow rate strongly influences the spectrum in short exposures. As can be seen in Fig. 3(a), just one, wide peak is present when $Cs_{35}NaX$ is saturated for 5 min at the high H_2S flow rate (40 cm^3 min^{-1}, curve A), while two peaks appear at the low rate (5 cm^3 min^{-1}) (curve B). Minor differences are observed when the contact is for 30 min at 40 and 5 cm^3 min^{-1} (curves C and D).

The influence of the saturation and purging temperature was also assessed. In Fig. 3(b), the usual desorption curve for $Cs_{26}NaX$ saturated and purged at 423 K (curve A) is compared with that obtained at 523 K (curve B), where the adsorption line is so broad that the first peak is virtually confused with the baseline. However, if the sample is first saturated at either 523 or 623 K, cooled to 423 K in flowing helium, and then purged at this temperature, both are clearly visible (curves C and D), and there is a close resemblance to curve A.

The following assumptions can be made to explain these results. The adsorbing H_2S molecule can interact with the solid via two pathways: one between the electron pair of the sulphur atoms and the alkali-metal cations, the other involving H_2S protons and lattice oxygens.

A similar situation seems to occur even when benzene is adsorbed on alkali-metal zeolites. De Mallmann and Barthomeuf [13,14], used IR methods to show that benzene adsorbs through its π electrons on cationic sites and its hydrogens on oxygen sites; here it is regarded as a slightly acid molecule interacting with the framework oxygens that act as the basic centres. Both types of interaction are present at the same time. Their prevalence will depend on the relative strengths of the acid and basic sites. δ_O [15–18] increases with the aluminium content for a given alkali-metal cation. In keeping with the general behaviour of acids and bases, the strength of the conjugated acid site on the solid, i.e. the alkali-metal cation, must also decrease at the same time.

A stronger interaction between non-dissociated H_2S and Na^+ cations should thus be expected on NaY ($\delta_O = -0.349$, Table 1) rather than NaX ($\delta_O = -0.399$). Indeed, we can see from Fig. 1 that the maximum of the TPD spectrum for NaY occurs at higher temperatures than that for NaX, i.e. the interaction of H_2S with NaX is weaker. Analogously, NaΩ ($\delta_O = -0.319$) has its maximum at a slightly higher temperature than NaY.

The amount of H_2S adsorbed by each sample (area under curve in Fig. 1) decreases as the Si/Al ratio increases, i.e. along the series NaX > NaY > NaΩ > silicalite. There is practically no adsorption on silicalite due to the virtual absence of Na^+ (0.03 wt.%).

IR studies of faujasites by Karge and co-workers [1–8] have shown simultaneous dissociative and non-dissociative adsorption for samples with Si/Al < 2.5, whereas dissociative adsorption did not occur at Si/Al > 2.5. This finding and the low δ_O value for NaΩ and NaY indicate that the TPD curves for these catalysts are initiated by non-dissociative adsorption (during saturation) only, while the sharp peak in the NaX spectrum is due to desorption of H_2S adsorbed both dissociatively and non-dissociatively. A δ_O value of -0.399 thus points to a situation where the lattice oxygens are basic enough to partly induce H_2S dissociation to H^+ and SH^-.

For a given structure and Si/Al ratio, δ_O can be varied by appropriate ion exchange. In our case, an increase in δ_O occurs as Cs^+ or Rb^+ ions progressively replace the Na^+ ions of NaX along the CsNaX and RbNaX series (Table 1). Their spectra, compared with that for NaX, are illustrated in Fig. 2. Figure 4 shows the plot of these temperature maxima versus δ_O. As can be seen, the temperature of the first maximum slightly decreases and then stabilizes, while the second maximum, which appears once δ_O reaches a threshold value of about -0.41, continuously shifts towards higher temperatures. For the CsNaX series, when the degree of ion exchange is low, no more than minor modification of the spectrum can be

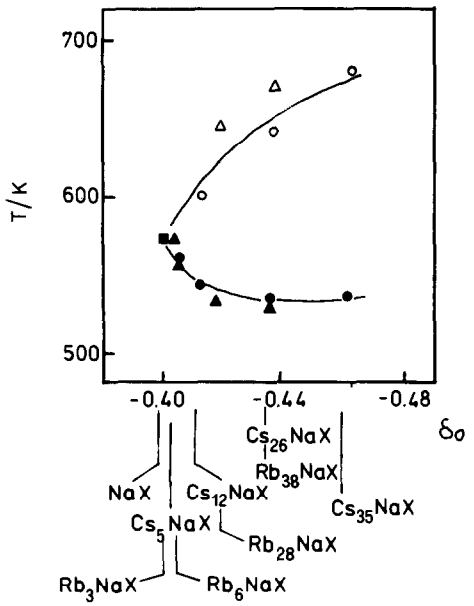

Fig. 4. Temperature of the maxima of the first peak (full symbols) and second peak (empty symbols) in TPD spectra of H_2S vs. negative charge of crystal lattice oxygen, δ_O. □, NaX; ○, CsNaX zeolites; △, RbNaX zeolites.

expected from the slight change in composition. Increasing amounts of Cs^+ increase the basicity of the lattice oxygens and enhance the dissociation of H_2S. H^+ will interact with oxygens, SH^- will compete with undissociated H_2S in its interaction with alkali-metal cations.

The Cs^+ ions are too big to enter the smaller cavities and are therefore located in the supercage. If we assume for our original NaX a cation distribution similar to that reported in the literature [19], a total exchange of the Na ions in the accessible supercages would correspond to $Cs_{44}NaX$. Thus, from NaX to $Cs_{35}NaX$, the samples should still contain Na^+ ions in the supercage together with Cs^+ ions in increasing amounts. Cs^+ ions are less acidic than Na^+ and should therefore interact more easily with the more basic SH^- species, than with H_2S. By contrast, H_2S should prefer the more acidic Na^+ cations for non-dissociative adsorption. These considerations suggest that the second peak, which appears in the spectra of the highly exchanged samples only, is related to the desorption of dissociatively adsorbed H_2S, as the strength of this interaction depends on the δ_O value and the amount of H_2S involved (area under the second peak) increases with the Cs^+ content. The first peak would reflect the interaction between the residual Na^+ ions in the supercage and the undissociated H_2S; accordingly, its area decreases with the average number of Na^+ ions in the big cavity. It can easily be shown that a similar reasoning also applies to the RbNaX series.

The simultaneous presence of both kinds of interaction on the same catalyst does not necessarily mean that they originate simultaneously. Figure 3(a) in fact reveals that the wide peak obtained after short exposure to H_2S at the higher flow rate (curve A) has its maximum in the typical region of non-dissociative interaction. Dissociative adsorption (i.e. the second peak) appears at low flow rate (curve B) when the first peak is markedly smaller. Under continuous flow operating conditions the extent of a reaction is determined (among other parameters) by the space-time value, i.e. for a given mass of solid, by the gaseous reactant flow rate. The higher the gaseous reactant flow rate, the lower the space-time value. The observed decrease of non-dissociative adsorption and the simultaneous establishment of dissociative adsorption (curve A compared with curve B) suggest that the latter interaction occurs consecutively to the first one, as if the lattice oxygens interact with the hydrogens of H_2S only when it has been non-dissociatively adsorbed. However, as we are under non-steady state conditions, the exposure time also plays a role. The higher its value the higher will be the extent of the reaction and the higher the amount of dissociatively adsorbed H_2S (compare curves A with C and B with D).

The spectra in Fig. 3(b) seem to support this idea: if the temperatures of both saturation and purging are high, the non-dissociative adsorption cannot occur, due to the high purging time, and thus no dissociation takes place. By contrast, cooling to 423 K after higher temperature saturation enables the sample to adsorb part of the H_2S adsorbed reversibly at 523 or 623 K and not yet purged, and dissociation occurs.

Furthermore, this picture seems to be in line with our previous findings on the catalytic behaviour of NaX [10]. When this catalyst was pretreated with MF before admitting H_2S, a dramatic decrease in both conversion and selectivity was observed. Partial saturation of the solid by MF could make it very difficult for H_2S to be adsorbed and then dissociated, as required for catalysis of the reaction.

TPD of MF

Some runs were performed on NaX, K_{70}NaX, Rb_{38}NaX and Cs_{35}NaX. The curves (Fig. 5a) stop at 623 K, since the heating rate was cut off to avoid the probable decomposition of MF at higher temperatures. As the MF molecule is too large to enter the sodalite cages, the curves presumably reflect the interaction between the alkali-metal cations in the supercage and MF. This may involve the π electrons of the heterocyclic ring rather than the electron pair sitting on the oxygen, as suggested by our quantum-mechanical calculations performed for the very similar furan/NaY system [20].

The ability of the alkali-metal cation to attract electrons can be measured by the ratio between the ionization energy of the alkali-metal atom

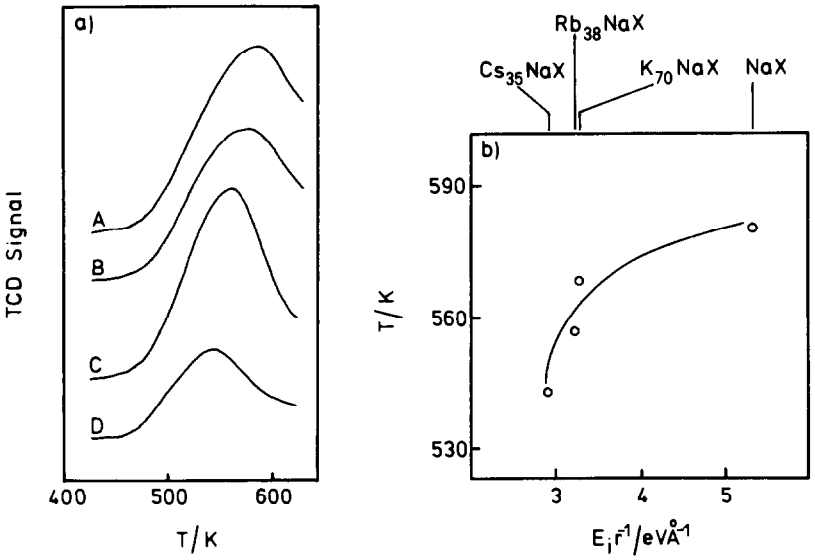

Fig. 5. (a) TPD spectra of MF for (A) NaX, (B) $K_{70}NaX$, (C) $Rb_{38}NaX$ and (D) $Cs_{35}NaX$; see text for saturation and purging conditions. (b) Temperature of the peak maximum in the TPD spectra of MF vs. $(E_i/r)_{av}$ for X zeolites of Fig. 5(a).

E_i and the radius r of the corresponding cation. When residual Na^+ ions are still present in the supercage besides the exchanging cations, i.e. in the case of $Rb_{38}NaX$ and $Cs_{35}NaX$, the following average parameter seems more appropriate

$$(E_i/r)_{av} = \frac{n_{Na}(E_i/r)_{Na} + n_{Me}(E_i/r)_{Me}}{n_{Na} + n_{Me}} \quad (1)$$

where n_{Na} and n_{Me} are the number of sodium and exchanging cations present in the supercage. Our values for this parameter are reported in Table 2. The increase in the strength of the interaction between the solid and MF expected along the series $Cs_{35}NaX < Rb_{38}NaX < K_{70}NaX < NaX$

TABLE 2

$(E_i/r)_{av}$ values [a] for the highly exchanged alkali-metal zeolites

Sample	n_{Na}	n_{Me}	r (Å)	E_i (eV)	$(E_i/r)_{av}$ (eV Å^{-1})
NaX	5.5		0.97	5.16	5.32
$K_{70}NaX$		5.5	1.33	4.33	3.26
$Rb_{38}NaX$	0.75	4.75	1.47	4.16	3.17
$Cs_{35}NaX$	1.1	4.4	1.69	3.90	2.91

[a] See text.

is demonstrated in Fig. 5(b), where the temperature of the maximum of each curve from Fig. 5(a) is plotted versus $(E_i/r)_{av}$.

CONCLUSIONS

The present results can be summarized as follows.

(1) The H_2S adsorption mode is governed by the acid–base character of the zeolite. Low δ_O values identify a situation where the adsorption is mainly non-dissociative (NaΩ, NaY). A progressive increase of the zeolite basicity, caused by a high aluminium content (NaX) and the presence of increasing amounts Cs^+ or Rb^+ ions (CsNaX and RbNaX zeolites), leads to the growing establishment of dissociative adsorption.

(2) When both the adsorption modes are possible, dissociation of H_2S appears to originate from non-dissociatively adsorbed H_2S.

ACKNOWLEDGEMENTS

Thanks are due to Ministero dell'Università e della Ricerca Scientifica e Tecnologica (M.U.R.S.T.) and Consiglio Nazionale delle Ricerche (C.N.R.), Rome, for financial support.

REFERENCES

1 H.G. Karge and J. Raskó, J. Colloid Interface Sci., 64 (1978) 522.
2 H.G. Karge, J. Ladebeck and N.K. Nag, in S.E. Wanke and S.K. Chakrabartty (Eds.), Preprints of Proc. 7th Canadian Symp. on Catalysis, Edmonton, Alberta, Canada, Oct. 1980. p. 225.
3 H.G. Karge and J. Ladebeck, in R. Sersale, C. Colella and R. Aiello (Eds.), Proc. 5th Int. Conf. on Zeolites, Recent Progress Reports and Discussion, Giannini, Naples, Italy, June 1980, p. 180.
4 M. Ziólek and Z. Dudzik, Zeolites, 1 (1981) 117.
5 H.G. Karge, Y. Zhang, S. Trevisan de Suares and M. Ziólek, in P.A. Jacobs, N.I. Jaeger, P. Jiru, V.B. Kazansky and G. Schultz-Ekloff (Eds.), Structure and Reactivity of Modified Zeolites, Elsevier, Amsterdam, 1984, p. 49.
6 A.B. Verver and W.P.M. Van Swaaij, Appl. Catal., 14 (1985) 185.
7 H.G. Karge, M. Ziólek and M. Laniecki, Zeolites, 7 (1987) 197.
8 M. Ziólek, J. Bresínska and H.G. Karge, Acta Phys. Chem. Szeged. Nova Set., 31 (1985) 551.
9 I. Ferino, R. Monaci, E. Rombi and V. Solinas, Thermochim. Acta, 135 (1988) 371.
10 I. Ferino, R. Monaci, E. Rombi and V. Solinas, Zeolites, 11 (1991) 64.
11 I. Ferino, R. Monaci and V. Solinas, C. Oliva, I. Pieri and L. Forni, J. Chem. Soc. Faraday Trans., 86(1) (1990) 193.
12 I. Ferino, R. Monaci and V. Solinas, C. Oliva, I. Pieri and L. Forni, J. Chem. Soc. Faraday Trans., 86(15) (1990) 2795.
13 A. De Mallmann and D. Barthomeuf, in Y. Murakami, A. Iijma and J.W. Ward (Eds.), New Developments in Zeolite Science and Technology, Kodanska, Tokyo, 1986, p. 609.
14 A. De Mallmann and D. Barthomeuf, Zeolites, 8 (1988) 292.

15 R.T. Sanderson, Science, 114 (1951) 670.
16 W.J. Mortier, J. Catal., 55 (1978) 138.
17 R.T. Sanderson, Chemical Bonds and Bond Energy, 2nd edn., Academic Press, New York, 1976.
18 W.J. Mortier, in P. Grobet, W.J. Mortier, E.F. Vansant and G. Schultz- Ekloff (Eds.), Innovation in Zeolites Material Science, Elsevier, Amsterdam, 1988, p. 253.
19 W.J. Mortier, Compilation of Extra Framework Sites in Zeolites, Butterworths, London, 1982.
20 M. Monduzzi, R. Monaci and V. Solinas, J. Colloid Interface Sci., 120 (1987) 8.